Chemical Engineering Journal 544 (2026) 178913

Contents lists available at ScienceDirect

Chemical Engineering Journal

journal homepage: www.elsevier.com/locate/cej

Stable single-membrane pH-decoupling aqueous all-organic flow batteries

Mingguang Pan [a,b], Zhong Jin [c], Jianwei Sun [a,d,e], Zhihu You [c], Alan Y.L. Fan [d], Minhua Shao [a,e,f,*]

[a] Department of Chemical and Biological Engineering, The Hong Kong University of Science and Technology, Clear Water Bay, Kowloon, Hong Kong, China
[b] School of Materials Science and Engineering, East China Jiaotong University, Nanchang, 330013, China
[c] State Key Laboratory of Coordination Chemistry, MOE Key Laboratory of Mesoscopic Chemistry, MOE Key Laboratory of High Performance Polymer Materials and Technology, Jiangsu Key Laboratory of Advanced Organic Materials, School of Chemistry and Chemical Engineering, Nanjing University, Nanjing, 210023, China
[d] Department of Chemistry, The Hong Kong University of Science and Technology, Clear Water Bay, Kowloon, Hong Kong, China
[e] Energy Institute, The Hong Kong University of Science and Technology, Clear Water Bay, Kowloon, Hong Kong, China
[f] Guangzhou Key Laboratory of Electrochemical Energy Storage Technologies, Fok Ying Tung Research Institute, The Hong Kong University of Science and Technology, Guangzhou, 511458, China

ARTICLE INFO

Keywords:
Aqueous all-organic flow batteries (AAOFBs)
Ammonium/amino-grafted bipyridiniums
pH-decoupling
Single-membrane
Hydrogen bonds

ABSTRACT

The advancement of pH-decoupling aqueous organic flow batteries (AOFBs) would enable high cell voltage and circumvent challenges in molecular engineering. However, traditional pH-decoupling AOFBs need the complicated three-chamber, two-membrane configuration and suffer from severe crossover issue. In the present work, stable pH-decoupling aqueous all-organic flow batteries (AAOFBs), separated with a single ion-exchange membrane, were first constructed by using the crossover-free NH_2/NH_3^+ grafted bipyridinium and N-heterocycle-linked TEMPO (TMP-TEMPO) redox pair. The bipyridiniums with NH_2/NH_3^+ terminals require minimal preparation steps and do not need an additional silica gel column. Notably, the NH_2 and NH_3^+ groups, being strong hydrogen bond acceptor and donor respectively, restrict free diffusion of proton and hydroxide ions through the low-cost Selemion AMVN anion-exchange membrane (AEM) and avoid their crossover contamination. Note that the Selemion AMVN AEM incorporates a polystyrene-based backbone with quaternary ammonium-functionalized side chains, which provides high ionic selectivity and chemical stability. As a consequence, stable single-membrane pH-decoupling AAOFBs at low concentration are demonstrated with an extremely low capacity fade rate of 0.22% per day over 638 cycles (~7 days), a high energy efficiency of ~88% and Coulombic efficiency of ~100%. The high-concentration pH-decoupling AAOFBs exhibited stable cycling performance even in a high O_2 content environment (100 ppm) with a practical capacity of 10.7 Ah L^{-1}, a capacity fade rate of 1.30% per day for 500 cycles, a Coulombic efficiency of ~99.8%, and an energy efficiency of 87%.

1. Introduction

The rapid deployment of renewable energy harvesting technologies has driven a significant demand for low-cost, sustainable, and durable stationary energy storage technologies [1]. Aqueous flow batteries (AFBs) are brilliant technologies capable of storing grid-scale electricity exceeding levels of MW/MWh [2]. AFBs are a class of unique rechargeable batteries in which the energy carriers are stored in the aqueous electrolytes and pumped to be circulated in each individual cell [3]. The marvelous configuration of AFBs enables a number of unique benefits, such as decoupled energy and power, excellent modularity and flexibility, and high intrinsic safety. Moreover, AFBs are easier to recycle and operate, as the electrolyte(s) can simply be refreshed, when compared to existing metal-based static batteries. Recently, aqueous organic flow batteries (AOFBs) comprising water-soluble organic electro-active materials (OEMs) in the electrolyte(s) are anticipated to be cost-effective and sustainable, since OEMs are composed of light, inexpensive, and abundant elements like carbon, hydrogen, oxygen, and nitrogen, and enable limitless molecular diversity and designability [4–29]. There are several groundbreaking works in establishing novel AOFBs under pH-acidic, −basic or -neutral conditions. For examples, the Wen's group and Narayanan's group pioneered novel organic flow

* Corresponding author at: Department of Chemical and Biological Engineering, The Hong Kong University of Science and Technology, Clear Water Bay, Kowloon, Hong Kong, China.
E-mail address: kemshao@ust.hk (M. Shao).

https://doi.org/10.1016/j.cej.2026.178913
Received 13 April 2026; Received in revised form 24 June 2026; Accepted 28 June 2026
Available online 30 June 2026

batteries based on quinone-based redox species in aqueous sulfuric acid solution, providing foundation for the development of AOFBs [4,5]. Aziz and his colleagues demonstrated the first alkaline quinone flow battery for cost-effective stationary energy storage [6]. In the meanwhile, Schubert et al. fabricated a pH-neutral, polymer-based flow battery using non-corrosive, safe and low-cost materials [7]. The Liu group designed asymmetrically substituted sulfonate viologens as capacity dense, chemically stable anolytes for pH-neutral AOFBs [8]. Liang et al. developed an electrochemical method to quantitatively investigate the aggregation behavior of bipyridiniums, demonstrating that the performance of AOFBs can be optimized by tuning their aggregation behavior [9,10]. Recently, Li's team established ultra-stable AOFBs using an in situ organic electrolysis strategy in a flow cell, providing an innovative approach for developing scalable, environmentally friendly, and cost-effective methods for creating redox-active materials [11,12]. Up to date, great attention was paid to the molecular engineering of electro-active materials for high-performance AOFBs, including high capacity, high voltage, and durable lifetime [13–29].

In most AOFBs, the pH levels of the positive and negative electrolytes are the same, making molecular engineering more challenging and limiting the range of available electro-active species. Therefore, a different pH environment between the two electrolytes (pH-decoupling) can significantly broaden opportunities for utilizing high-voltage redox molecules [30,31]. By using a three-chamber, two-membrane configuration, pH-decoupling AOFBs can achieve high voltage and power output [30]. However, the complex cell architectures with two different membranes significantly increase the cost. Additionally, the unavoidable crossover of protons or hydroxide ions may increase the energy required to recover the initial pH difference and result in short lifetime with fast capacity fade and low round-trip energy efficiency of AOFBs. To date, single-membrane pH-decoupling AAOFBs have not been demonstrated due to the challenges in electro-active materials, membranes and their compatibility issues (Table 1).

2. Experimental

2.1. Materials

The preparation of [TMP-TEMPO]Cl_2 was according to the synthetic procedures in our previous literature [29]. All reagents were purchased from commercial sources, stored in the refrigerator (2 °C) or in the desiccator, and used as received unless otherwise stated.

2.2. Preparation of $[(NH_3Pr)_2V]Cl_4$

The $[(NH_3Pr)_2V]Cl_4$ compound was prepared by two methods as follows. In the first method, 4,4′-bipyridine (1.5 g, 9.6 mmol), 3-bromopropylamine hydrobromide (4.336 g, 19.81 mmol) were mixed with 3 mL of H_2O in a high-pressure Schlenk flask (15 mL). The reaction mixture was sealed and stirred at 110 °C for 24 h. After the reaction mixture was cooled down to room temperature, it was poured into 60 mL of ethanol. The resulting precipitate was filtered and washed with ethanol and then acetone several times. The crude product was first dissolved in DMSO solvent, and then the resulting solution was mixed with an equivalent volume of an ethanol/acetone mixture (*v*/v, 1/2). As a result, the pure product $[(NH_3Pr)_2V]Br_4$ was precipitated as a yellow solid. Subsequently, the bromide ions of $[(NH_3Pr)_2V]Br_4$ were exchanged by chloride ions with an anion-exchange column (Amberlite IRA-900 (Cl) resin) to obtain $[(NH_3Pr)_2V]Cl_4$ as a white solid quantitatively with a NMR purity of ~100% (3.03 g, overall yield: 75.8%). In the second method, 4,4′-bipyridine (2.0 g, 12.8 mmol), 3-chloropropylamine hydrochloride (3.36 g, 25.8 mmol) were mixed with 3 mL of H_2O in a high-pressure Schlenk flask (15 mL). The reaction mixture was sealed and stirred at 110 °C for 48 h. After the reaction mixture was cooled down to room temperature, it was poured into 120 mL of methanol. The resulting precipitate was filtered and washed with methanol several times. The crude product contains a small amount of monosubstituted impurities. The crude product is almost not dissolved in the common solvents such as DMSO and DMF, making the further purification in difficulty. Thus, the NMR purity of $[(NH_3Pr)_2V]Cl_4$ is 94% ~ 96%. ^{1}H NMR (400 MHz, D_2O, room temperature) = 9.06 (d, J = 6.83 Hz, 4H), 8.47 (d, J = 6.75 Hz, 4H), 4.74 (t, J = 7.80 Hz, 4H), 3.07 (t, J = 7.85 Hz, 4H), 2.42–2.34 (m, 4H). ^{13}C NMR (100 MHz, D_2O, room temperature) = 149.7, 145.0, 126.7, 58.1, 35.5, 27.7.

2.3. Preparation of $[(NH_2Pr)(NH_3Pr)V]Cl_3$ and $[(NH_2Pr)_2V]Cl_2$

For all battery tests, $[(NH_2Pr)(NH_3Pr)V]Cl_3$ and $[(NH_2Pr)_2V]Cl_2$ electrolytes were obtained by neutralizing $[(NH_3Pr)_2V]Cl_4$ electrolytes with one and two equivalents of NaOH, respectively. For solubility tests, $[(NH_2Pr)(NH_3Pr)V]Br_3$ was obtained by neutralizing $[(NH_3Pr)_2V]Br_4$ with one equivalent of NaOH in water. The resulting $[(NH_2Pr)(NH_3Pr)V]Br_3$ solution was dried on a rotary evaporator to remove any residual water, washed with methanol to eliminate any possible NaBr, and then dried under vacuum. Subsequently, the bromide ions of $[(NH_2Pr)(NH_3Pr)V]Br_3$ were exchanged by chloride ions with an anion-exchange column (Amberlite IRA-900 (Cl) resin) to obtain $[(NH_2Pr)(NH_3Pr)V]Cl_3$. $[(NH_2Pr)_2V]Cl_2$ could not be completely dried due to its instability in the air. Thus, only its crude solubility is obtained (see Solubility test, as below).

2.4. Solubility test

The solubilities of $[(NH_3Pr)_2V]Cl_4$ and $[(NH_2Pr)(NH_3Pr)V]Cl_3$ were determined using UV–vis spectroscopy [32]. The experimental procedure for measuring solubility was as follows: First, a 5 mM sample was dissolved in 5 mL of aqueous solution (either water or 2 M NaCl) and then diluted to concentrations of 5, 10, 15, 20, and 25 μM. Second, a standard curve was established based on the UV–vis spectroscopy measurements of these concentrations. Third, the saturated aqueous solution was prepared by adding solvent until complete dissolution, followed by progressive dilution up to 125,000 times (10 μL of the saturated solution was diluted to 5 mL, and then 20 μL of this solution was further diluted to 5 mL). As a result, the saturated concentration (i.e., solubility) of the sample was calculated. We measured the crude solubility of the $[(NH_2Pr)_2V]Cl_2$ sample using a simple method as the neat and completely dried sample is unstable and difficult to obtain. First, we weighed 416.21 mg $[(NH_3Pr)_2V]Cl_4$ and added 500 uL of 4 M NaOH to a 5 mL graduated measuring cylinder. After fully mixing, we diluted the reaction mixture with H_2O to 1 mL, resulting in a clear and

Table 1
Battery performance comparison with all the pH-decoupling semi- or all-organic AFBs in previous literature.

Ref	Redox pair	Membrane	Capacity (Ah L^{-1})	Life time (h)	Fade rate (% d^{-1})
This work	$[(NH_2Pr)(NH_3Pr)V]Cl_3$, $[TMP\text{-}TEMPO]Cl_2$	Selemion AMVN	2.4	166.3	0.22
			10.7	436.8	1.30
[30]	BHPC, $Fe(Bhmbpy)_3$	Fumasep E620/Selemion DSVN	2.81	432	0.07
[30]	KCrPDTA, KBr/KBr_3	Nafion 212	25	18	5.33
[31]	$Zn/Zn(OH)_4^{2-}$, FQH_2/FQ	Nafion 117/Selemion DSV	4.5	42	2.22

homogeneous solution. Thus, the solubility of $[(NH_2Pr)_2V]Cl_2$ should be >1 M in 2 M NaCl aqueous solution.

2.5. Electrochemical analysis

Electrochemical experiments, including cyclic voltammetry (CV) and linear sweep voltammetry (LSV), were conducted in a three-electrode glass cell. The setup comprised a glassy carbon electrode as the working electrode, a Pt wire as the counter electrode, and an Ag/AgCl electrode as the reference, all in 0.5 M NaCl electrolyte solutions. Prior to experimentation, the glassy carbon working electrode was polished with Al_2O_3 (30 nm diameter) suspended in deionized water, followed by rinsing and drying with airflow. CV and LSV experiments were performed using a CHI760, CHI660E, or CHI627e workstation (CH Instruments), with all potentials referenced to SHE based on the known $MV^{2+/1+}$ redox couple (−0.45 V vs SHE). A 3 mm glassy carbon electrode (GC 130) was used as the working electrode in CV measurements, while a 5 mm glassy carbon rotating disk electrode was used as the working electrode in LSV measurements. During the LSV tests, the disk electrode rotated from 300 rpm to 2400 rpm in increments of 300 rpm. LSV scans were obtained at a rate of 5 mV s^{-1} from 0 V to −0.95 V versus SHE.

The diffusion coefficient (D) values were derived from the corresponding linear slopes, using the Levich equation as follows:

$$i_{Lim} = 0.62nFAcD^{2/3}\upsilon^{-1/6}\omega^{1/2} \quad (1)$$

Here, i_{Lim} denotes the limiting current, n represents the number of electrons transferred ($n = 1$ for each electron), F is Faraday's constant (96,485C mol^{-1}), A is the electrode area (0.1963 cm^2), c is the concentration of the redox-active material (1×10^{-6} mol cm^{-3}), υ is the kinematic viscosity of a 0.5 M NaCl solution (0.009 cm^2 s^{-1}), and ω denotes the rotation rate.

Furthermore, the Koutecký-Levich and Tafel equations were used to calculate the kinetic rate constant (k_0) values:

$$i_m^{-1} = i_k^{-1} + B_L^{-1}\omega^{-1/2} \quad (2)$$

$$log_{10}|i_k| = log_{10}|nFcAk_0| + \frac{\alpha nF|E - E^{0\prime}|}{2.303 \times RT} \quad (3)$$

The parameters including ω, n, F, c, and A are defined in eq. (1), i_m denotes the measured current, i_k represents the kinetic current, B_L is the Levich constant, α is the charge transfer coefficient, $|E\text{-}E^{0\prime}|$ is the absolute difference between the measured potential (E) and the formal potential ($E^{0\prime}$), R is the universal gas constant (8.314 J K^{-1}), and T represents the temperature at 293.15 K.

2.6. Flow cell assemblies

To assemble the flow cell, two graphite electrolyte chambers, two graphite felt electrodes, a piece of anion-exchange membrane (AMVN, 100 μm thickness, Selemion, Japan) sandwiched between graphite felts, and two titanium current collectors were used. A piece of PTFE tubing was used to connect each graphite chamber to an electrolyte reservoir. The graphite felt (CeTech GF) had an area of 5 cm^2. A two-channel peristaltic pump (Longer Pump WT600-2 J) was used to press a Viton tubing and circulate electrolytes through the electrodes at a flow rate of 60 mL/min. For low electrolyte concentration, the anolyte reservoir contained 4.5 mL or 5 mL or 5.5 mL of 0.1 M bipyridinium in 2.0 M NaCl aqueous solution, and the catholyte reservoir contained 7 mL or 7.5 mL or 8 mL of 0.1 M $[TMP\text{-}TEMPO]Cl_2$ in 2.0 M NaCl aqueous solution (in excess). For high electrolyte concentration, 5 mL of 0.5 M bipyridinium in 2.0 M NaCl aqueous solution, 7.5 mL of 0.5 M $[TMP\text{-}TEMPO]Cl_2$ in 2.0 M NaCl aqueous solution were used for flow cell test. Note that in this work, the bipyridinium can be $[(NH_3Pr)_2V]Cl_4$, $[(NH_2Pr)(NH_3Pr)V]Cl_3$ or $[(NH_2Pr)_2V]Cl_2$. The flow battery was galvanostatically charged to 1.55 V or 1.6 V and discharged to 0.9 V at room temperature at a current density of 20 mA/cm^2.

2.7. Theoretical calculation

The Gaussian 09 software package was employed for all DFT calculations. Geometrical structure optimizations were conducted in the gas phase using the B3LYP functional with a 6-311G (d, p) basis set. The optimized structures were checked by their harmonic vibrational frequencies to ensure that they were at the potential energy surface minima with the number of imaginary frequencies equaling 0.

The theoretical volumetric density of the AORFB is calculated using the equation:

$$\text{Theoretical volumetric capacity} = 26.806 \times nc\ \left(\text{Ah L}^{-1}\right) \quad (4)$$

Here, n is the electron number per molecule, c is the molecular concentration (M).

3. Results and discussion

3.1. Molecular engineering principles and materials preparation

In this study, the bipyridinium backbone was functionalized with NH_3^+ and NH_2 terminals ($[(NH_3Pr)(NH_2Pr)V]Cl_3$) using minimal preparation steps without requiring a silica gel column. The simple molecular design not only induced the formation of charge distribution asymmetry but also offered hydrogen bonding donor and acceptor sites. The NH_2 group, being a strong hydrogen bond acceptor, is capable of trapping protons from water. On the other hand, the NH_3^+ group, being a strong hydrogen bond donor, can provide protons to form hydrogen bonds with water. The strong proton trapping capability of NH_2 with water resulted in restricted free diffusion of hydroxide ions and avoided the crossover contamination of hydroxide ions. Moreover, the pH-decoupling electrolytes with the alkaline anolyte and neutral catholyte largely inhibit the hydrogen evolution in the anolyte and the oxygen evolution in the catholyte. The noteworthy feature of NH_2/NH_3^+ grafted bipyridiniums facilitates the establishment of stable pH-decoupling AAOFBs using a commercially available anion-exchange membrane. As a proof of concept, the proton trapping strategy via molecular engineering can be extended to develop low-cost, single-membrane, and mild pH-decoupling AAOFBs. In addition, by regulating the O_2 content, the impact of O_2 on bipyridinium-based AAOFBs at low and high electrolyte concentrations was well understood. As a consequence, the assembled pH-decoupling AAOFBs at 0.1 M electron concentration demonstrated very impressive battery performance with a discharge capacity of ~2.4 Ah L^{-1}, capacity retention rate of ~99.998% per cycle over 638 cycles (capacity retention rate of 0.22% per day), and high energy efficiency of ~88% and Coulombic efficiency of ~100%. The high concentration pH-decoupling AAOFBs achieved a practical capacity of ~10.7 Ah L^{-1} with a capacity fading rate of 1.30% per day over 500 cycles during a ~ 436.8 h test in an AAOFB cell. Moreover, the high concentration AAOFBs are tolerant to high level of O_2 (100 ppm), enabling stable cycling without a drop of Coulombic efficiency.

The variation of Coulomb repulsion can directly influence aggregation behavior, such as π-dimerization, which plays an important role in battery performance. Bipyridiniums with multiple positive charges, such as BTMAP-Vi in previous literature [33], commonly decompose during long-term battery cycling due to excessive Coulomb repulsion, which can cause molecular collapse. Although traditional molecular engineering can tune the strength of Coulomb repulsion, it often requires complicated synthesis procedures. Once a molecule is designed with conventional covalent bonds, its molecular charges become fixed and difficult to modify [9]. It is a significant challenge to minimize the synthesis steps while regulating the Coulomb repulsion and π-dimerization in a dynamic and flexible way. Therefore, in our bipyridinium

system, Coulomb repulsion and π-dimerization can be flexibly and dynamically regulated by varying the charges through the protonation and deprotonation of amino terminals with simply adding an acid or base. The resultant charge asymmetry of $[(NH_3Pr)(NH_2Pr)V]Cl_3$ plays a crucial role in regulating intra-/inter-molecular Coulomb repulsions, altering the degree of π-dimerization, and ensuring high water solubility.

The bipyridiniums were easily prepared under mild conditions with only two or three synthetic steps without the need for a silica gel column. Briefly, $[(NH_3Pr)_2V]Cl_4$ was prepared via the reaction of 4,4′-bipyridine and 3-bromopropylamine hydrobromide at a molar ratio of 1:2.06 in water in a sealed flask at 110 °C for 24 h, followed an anion exchange from bromide to chloride (a two-step synthetic method), with an overall yield of ~76% and ultra-high NMR purity of ~100% (Fig. S1). Another synthetic method (a one-step synthetic method) is that, 4,4′-bipyridine can also directly react with 3-chloropropylamine hydrochloride to afford $[(NH_3Pr)_2V]Cl_4$ with a yield of 78% and a high NMR purity of 94–96% (Fig. S2). The $[(NH_3Pr)_2V]Cl_4$ using both synthetic methods can be easily obtained on a gram-scale. Among all the existing bipyridiniums, our bipyridiniums are among the most cost-effective and sustainable examples. The slightly different synthetic procedures and purities have no obvious impact on the performance of AAOFBs. Subsequently, $[(NH_3Pr)_2V]Cl_4$ reacted with one or two equivalent amounts of NaOH through an acid-base neutralization reaction, yielding $[(NH_2Pr)(NH_3Pr)V]Cl_3$ or $[(NH_2Pr)_2V]Cl_2$ quantitatively. To better clarify the redox reaction mechanism, bipyridiniums with ~100% NMR purity via the two-step synthetic method were used for battery performance testing and mechanism analysis.

3.2. Characterization of physicochemical and electrochemical properties

These NH_2 or NH_3^+ grafted bipyridiniums have high solubilities in aqueous solutions. For instance, based on titration using UV–Visible absorption spectroscopy [32], $[(NH_3Pr)_2V]Cl_4$ has solubilities of 1.8 M and 1.66 M in H_2O and 2 M NaCl, respectively (Fig. 1b, Fig. S3). Similarly, $[(NH_2Pr)(NH_3Pr)V]Cl_3$ exhibits high solubilities of 1.77 M and 1.78 M in H_2O and 2 M NaCl, respectively (Fig. 1b, Fig. S4). The demonstrated solubilities are competitive to those of other bipyridiniums in the literature. However, it is difficult to accurately determine the aqueous solubility of $[(NH_2Pr)_2V]Cl_2$ because its dried form is susceptible to oxidation or decomposition. Based on another solubility test method (see the supporting information), its solubility in 2 M NaCl is measured to be >1 M. By coupling with the crossover-free *N*-heterocycle-substituted TEMPO (TMP-TEMPO), a high cell voltage of ~1.38 V was demonstrated using the first redox reaction of $[(NH_2Pr)(NH_3Pr)V]Cl_3$ (Fig. 1c).

The proton-switchable behavior of these bipyridiniums results in a charge shift between symmetry and asymmetry (Fig. 2a). The titration of a 0.1 M solution of $[(NH_3Pr)_2V]Cl_4$ indicates the presence of two protons in the molecule, and suggests a p*K*a value of approximately 9 (Fig. 2b). As more protons are lost from $[(NH_3Pr)_2V]Cl_4$, the ^1H NMR chemical shifts move towards the upfield region (lower chemical shift, Fig. 2c), which is attributed to an increase in electron density. The ^1D NOESY NMR spectra reveal that the hydrogen atoms in all these bipyridiniums exhibit consistent spatial correlations, indicating a linear conformation regardless of proton loss or gain (Fig. 2d).

The redox chemistry of these bipyridiniums was confirmed to be the

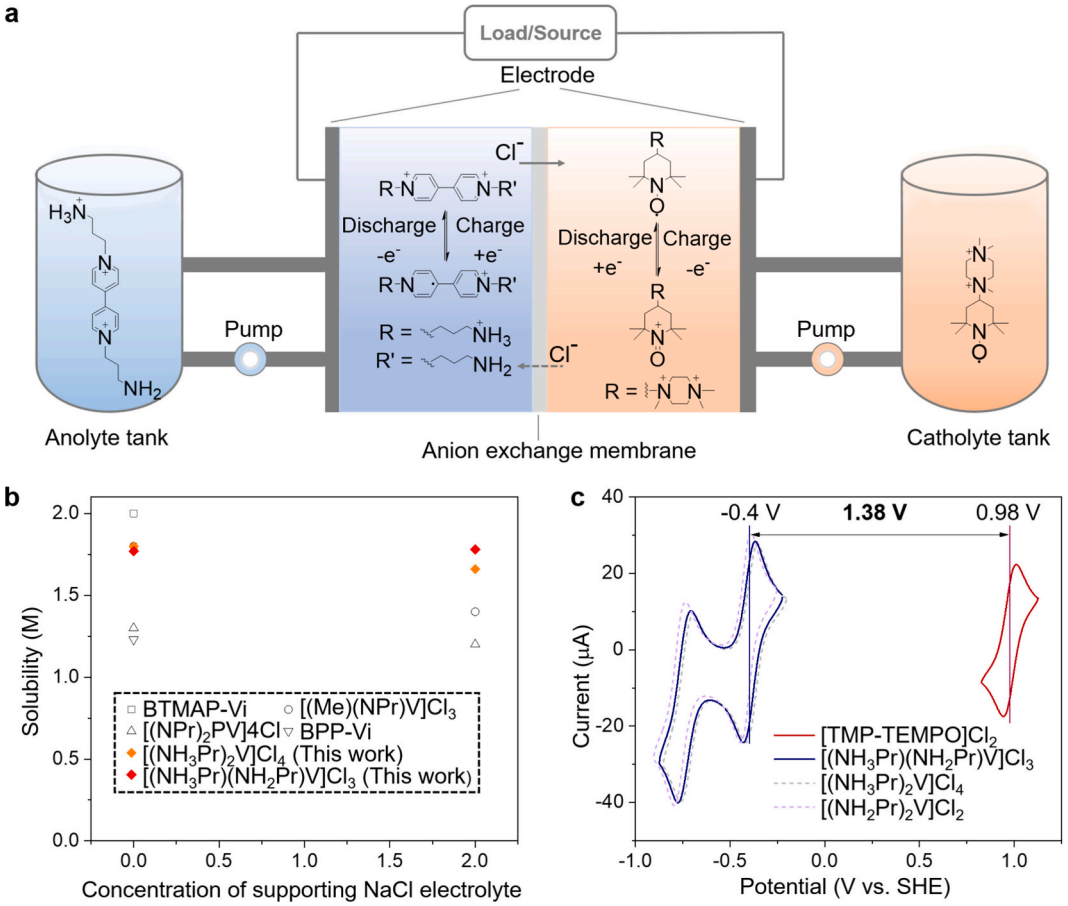

Fig. 1. (a) Schematic configuration of the pH-decoupling AAOFB and its anodic and cathodic redox reactions. (b) Solubility comparison of $[(NH_3Pr)_2V]Cl_4$ and $[(NH_2Pr)(NH_3Pr)V]Cl_3$ with the representative reported viologen analogues. (c) CV curves of 2 mM $[(NH_3Pr)_2V]Cl_4$, $[(NH_2Pr)(NH_3Pr)V]Cl_3$, $[(NH_2Pr)_2V]Cl_2$ and 2 mM $[TMP\text{-}TEMPO]Cl_2$ in a 0.5 M NaCl aqueous solution at a scan rate of 100 mV s^{-1}.

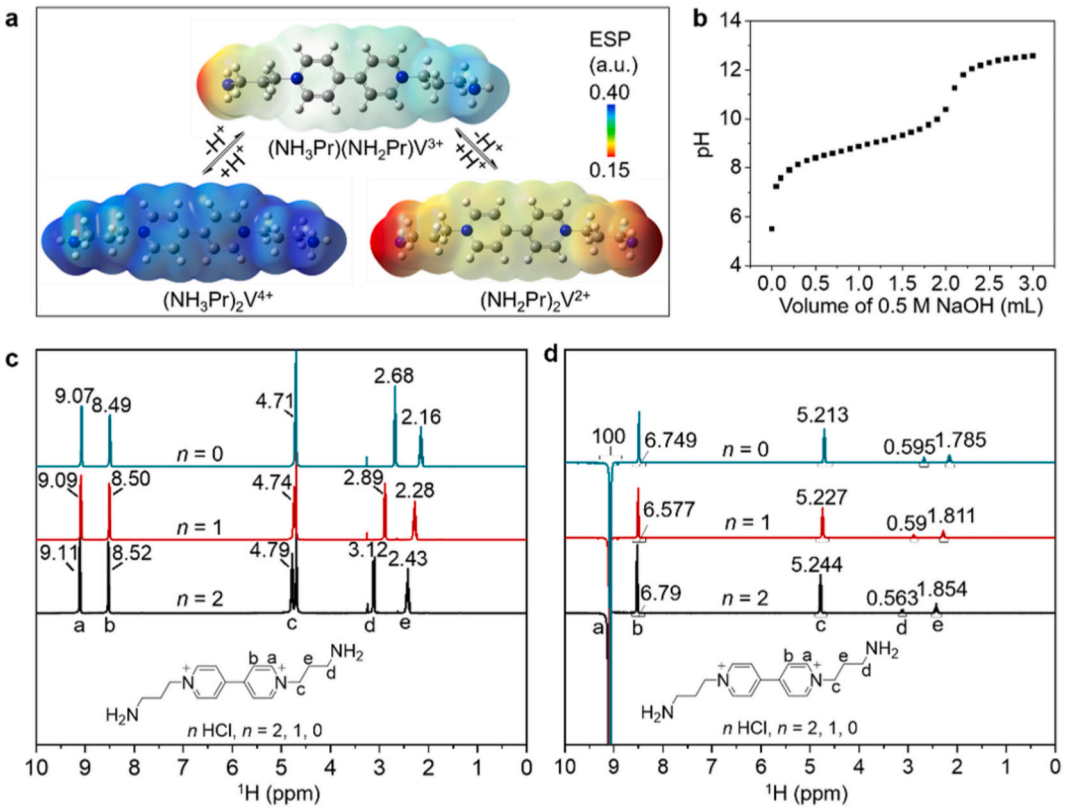

Fig. 2. (a) Calculated electrostatic potential (ESP) distributions of $[(NH_3Pr)_2V]Cl_4$, $[(NH_2Pr)(NH_3Pr)V]Cl_3$ and $[(NH_2Pr)_2V]Cl_2$. (b) Titration of 5 mL 0.1 M $[(NH_3Pr)_2V]Cl_4$ with 0.5 M NaOH showing the p*K*a of ~9. (c) ^{1}H NMR spectra (D_2O, room temperature) of $[(NH_3Pr)_2V]Cl_4$, $[(NH_2Pr)(NH_3Pr)V]Cl_3$ and $[(NH_2Pr)_2V]Cl_2$. (d) ^{1}D NOESY spectra of $[(NH_3Pr)_2V]Cl_4$, $[(NH_2Pr)(NH_3Pr)V]Cl_3$ and $[(NH_2Pr)_2V]Cl_2$.

two single-electron redox reactions by cyclic voltammetry (CV) curves under different pH conditions (Fig. 3a, b). Cyclic voltammograms and corresponding Pourbaix diagrams obtained by measuring the redox potentials at different pH values revealed that both the first and second redox potentials remained nearly unchanged from pH 3.62 to 7.13 and from pH 11.51 to 12.59, indicating that the two single-electron processes did not involve protons in this pH regions. In the mild alkaline solution (pH from 8.27 to 9.83), both the first and second redox potentials shifted towards the negative direction with a slope of −0.019 V/pH and of −0.023/pH, respectively. This shift can be attributed to an increase in molecular electron density during the proton loss from the NH_3^+ terminal(s). The reversible CV curves obtained from pH 3.62 to 12.59 indicate that our designed bipyridiniums are suitable in a wide pH range from acidic to alkaline conditions for AAOFBs.

The electrochemical properties of $[(NH_2Pr)(NH_3Pr)V]Cl_3$ were investigated by CV tests at different scan rates and by rotating disk electrode (RDE) tests with different rotation speed. CV profiles of $[(NH_2Pr)(NH_3Pr)V]Cl_3$ at scan rates of 20–100 mV s^{-1} indicated reversible and diffusion-controlled redox processes, as demonstrated by the linear correlation between peak current (i_p) and square root of scan rate ($\nu^{1/2}$) (Fig. S5). There is a positive correlation between the redox potential polarization and the scan rate. Moreover, RDE tests based on linear sweep voltammetry (LSV) were conducted (Fig. 3c, d), yielding the diffusion coefficient (D) and kinetic rate constant (k_0). The linear Levich plot using the limiting current (i) and the square root of the rotation speed ($\omega^{1/2}$) produces a D value of $(3.94 \pm 0.05) \times 10^{-6}$ cm^2 s^{-1} and of $(4.76 \pm 0.06) \times 10^{-6}$ cm^2 s^{-1} for the first and second reductions of $[(NH_2Pr)(NH_3Pr)V]Cl_3$, respectively. Using the Koutecký–Levich and Tafel equations, the k_0 values of $(3.12 \pm 0.02) \times 10^{-2}$ cm s^{-1} and $(3.50 \pm 0.02) \times 10^{-2}$ cm s^{-1} were obtained for the first and second redox reactions, respectively (Fig. S6).

3.3. Flow battery performance

The pH-decoupling AAOFBs based on the $[TMP\text{-}TEMPO]Cl_2$ catholyte and the NH_2 or NH_3^+ grafted bipyridiniums anolytes were assembled and separated by a single anion-exchange membrane (Selemion AMVN). The charging cut-off voltage was set to 1.55 V or 1.6 V for only use of the first redox potentials of these bipyridiniums. As shown in Fig. 1c and Fig. S7, the cell voltages of these AAOFBs increased with an increase in the deprotonation of $[(NH_3Pr)_2V]Cl_4$. This is because the ammonium deprotonation leads to an increase of molecular electron density and a negative redox potential shift. The $[(NH_3Pr)_2V]Cl_4$/[TMP-TEMPO]Cl_2 AAOFB with 0.1 M electron concentration was constructed and delivered the discharge capacity of ~1.75 Ah L^{-1} (Fig. S8). There is a capacity fluctuation from the 80th to 150th cycles, which should be induced by the pH fluctuation in the anolyte. Then the capacity increased to ~1.9 Ah L^{-1} and remained relatively stable in the subsequent cycles. Trace amount of O_2 can induce the disproportionation reaction of bipyridinium radical and generate additional hydroxide ions to neutralize the proton(s) on the NH_3^+ terminal of bipyridinium. Therefore, the $[(NH_3Pr)_2V]Cl_4$ anolyte after cycling became alkaline with a pH value of ~9, likely due to the O_2 triggered disproportionation and deprotonation. Inspired by this interesting battery phenomenon, the acidic $[(NH_3Pr)_2V]Cl_4$ was neutralized with an equivalent amount of NaOH to generate $[(NH_2Pr)(NH_3Pr)V]Cl_3$ with a p*K*a value of ~9. The $[(NH_2Pr)(NH_3Pr)V]Cl_3$ anolyte with mild alkalinity enabled stable cycling battery performance with a discharge capacity of 2.14 Ah L^{-1}, capacity fade rate of <0.5% per day (capacity retention of 97.2% over 688 cycles), high Coulombic efficiency of ~100% and high energy efficiency of ~86% (Fig. S9). The loss of two protons from $[(NH_3Pr)_2V]Cl_4$ created $[(NH_2Pr)_2V]Cl_2$ with strong alkalinity. The AAOFB based on $[(NH_2Pr)_2V]Cl_2$ anolyte allowed for comparable discharge capacity, Coulombic efficiency and energy efficiency but with a faster capacity

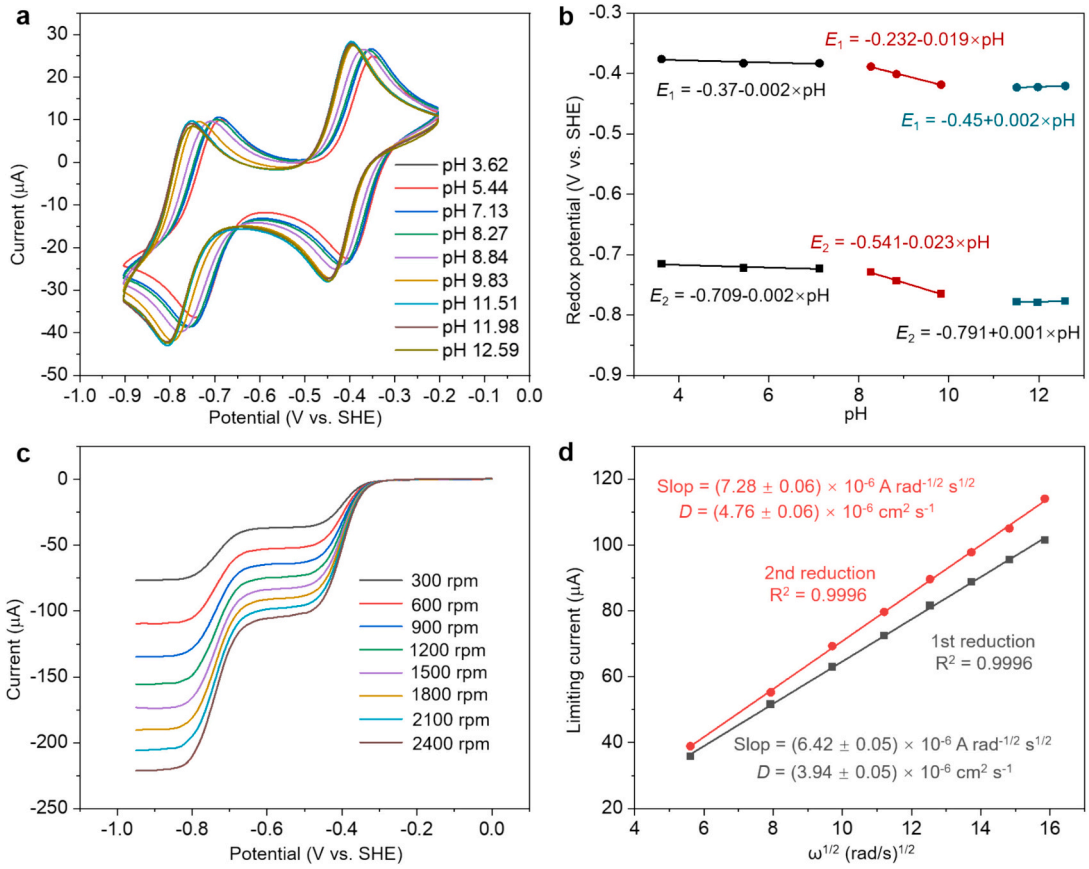

Fig. 3. (a) Cyclic voltammograms (scan rate = 100 mV s^{-1}) of 2 mM $[(NH_3Pr)_2V]Cl_4$ in a 0.5 M NaCl solution on a glassy carbon electrode at various pH conditions. The pH of the solutions was adjusted by adding appropriate amounts of HCl or NaOH, and the resulting pH values were measured using a pH potentiometer. (b) The corresponding Pourbaix diagrams for $[(NH_3Pr)_2V]Cl_4$. (c) LSV curves of 1.0 mM $[(NH_2Pr)(NH_3Pr)V]Cl_3$ in a 0.5 M NaCl solution with a scan rate of 5 mV s^{-1} at different rotation speeds from 300 to 2400 rpm. (d) The corresponding Levich plots of limiting current vs. square root of rotation rate ($\omega^{1/2}$) for $[(NH_2Pr)(NH_3Pr)V]Cl_3$.

degradation rate of ~1.7% per day as compared to $[(NH_2Pr)(NH_3Pr)V]Cl_3$ (Fig. S10). After the cycling, all AAOFBs showed no visible pH change in the TMP-TEMPO catholytes when compared to the fresh TMP-TEMPO catholytes, indicating the negligible crossover of proton or hydroxide ion from the anolyte. This is because the NH_2 group as a hydrogen bond acceptor and NH_3^+ group as a hydrogen bond donor, can form strong hydrogen bonds with water and avoid the proton or hydroxide ion crossing into the catholyte. Moreover, no crossover contamination of redox active species was found (Fig. S11). Therefore, as a proof of concept, stable single-membrane pH-decoupling aqueous organic flow batteries were successfully constructed.

Furthermore, the impact of O_2 on the single-electron AAOFB was investigated. Up to date, the impact of O_2 on the single-electron bipyridinium based AAOFB is not clear. In our common sense, the single-electron bipyridinium radical is highly sensitive to oxygen and prone to disproportionation in the presence of O_2, leading to a continuous capacity fade of AAOFB. Surprisingly, we found that increasing the oxygen content within a reasonable time had a positive effect on the capacity of AAOFB at diluted electrolyte concentrations (Fig. 4). Specifically, the AAOFB demonstrated stable battery performance over approximately 270 cycles without any capacity drop in a low O_2 content of 10 ppm. Afterwards, the capacity of AAOFB slightly decreased from 2.4 Ah L^{-1} to 2.27 Ah L^{-1} when further prolonged to 450 cycles. This capacity decay is likely caused by the strong formation of π dimers, which are reinforced by π-radical interactions and intermolecular hydrogen bonds. Interestingly, after 450 cycles, when the oxygen content in the atmosphere increased to 100 ppm, the capacity of AAOFB rapidly recovered to 2.38 Ah L^{-1} in the next 40 cycles, albeit with a slight decrease in Coulombic efficiency from 99.9% to 99.7% as depicted

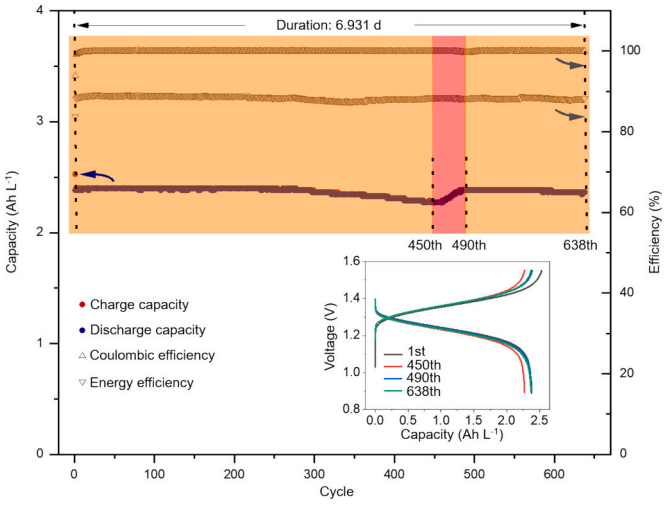

Fig. 4. Low-concentration cycling performance with the charging cut-off voltage of 1.55 V via N_2 content control, showing charge capacity, discharge capacity, Coulombic efficiency and energy efficiency vs cycle number. Orange region: in N_2 99.999%. Red region: in N_2 99.99%. Inset: typical galvanostatic charge-discharge profiles. Conditions: anolyte, 5.5 mL of 0.1 M $[(NH_2Pr)(NH_3Pr)V]Cl_3$ in 2.0 M NaCl solution; catholyte, 8 mL of 0.1 M [TMP-TEMPO]Cl_2 in 2.0 M NaCl solution; current density, 20 mA cm^{-2}.

in Fig. 4 (red region) and Fig. S12. This intriguing battery phenomenon aligns with findings from a Nature journal article, which demonstrates that the O_2 content can positively affect battery capacity, suggesting slow O_2 reduction and low accumulation of peroxides [34]. As a result, the O_2 level increased from 10 ppm to 100 ppm, leading to a slight decrease in Coulombic efficiency. After 490 cycles, the O_2 content in the atmosphere was once again reduced to 10 ppm to prevent O_2-induced competing side reactions, resulting in the recovery of Coulombic efficiency (Fig. S12). The battery can further run for at least 100 cycles with no obvious capacity drop in an environment with 10 ppm O_2. By such round-trip N_2 regulation, the pH-decoupling AAOFBs facilitate stable cycling performance with a discharge capacity of 2.4 Ah L^{-1}, capacity retention of ~98.5% for the whole consecutive 638 cycles (a capacity fade rate of 0.22% per day or 0.00235% per cycle), and high energy efficiency of ~88% and Coulombic efficiency of ~100%. The reproducible results demonstrated that O_2 has both favorable and unfavorable impacts on battery capacity in dilute concentration AAOFBs, challenging the conventional belief in the incomparability between the single-electron bipyridinium radical and O_2. This study provides new insights that an ultra-low level of O_2 (<10 ppm) may not always be necessary for bipyridinium radicals to exhibit stable battery performance. In addition, it is important to note that even with the same concentration and volume of redox species, slight micro-structure and thickness variations in the Selemion AMVN anion-exchange membrane (AEM) can cause discharge volumetric capacities to differ somewhat (Fig. 4 and Figs. S9, S10). The capacity shown in Fig. 4 differs from that in Fig. S9 or S10 because of a membrane refresh, despite both membranes being of the same type. It is worth mentioning that the Selemion AMVN AEM is made from hydrocarbon polymers with quaternary ammonium-functionalized side chains that prevent the crossover of bipyridiniums grafted with NH_3^+ or NH_2 terminals and provide chloride or hydroxide conductivity. Thanks to its polystyrene-based backbone, this type of AEM exhibits excellent chemical stability and resistance to chain cleavage even under high pH conditions, thereby enabling stable single-membrane pH-decoupling AAOFBs. Recently, AEMs made from a rigid *p*-terphenyl polymer framework with piperidinium side groups have demonstrated excellent alkaline stability due to their robust chemical structure, making them potentially suitable for the AAOFB system developed in this study [35–37].

Moreover, the high concentration pH-decoupling AAOFB was conducted using the Selemion AMVN AEM (Fig. 5). The AAOFB demonstrated a high volumetric capacity of 10.7 Ah L^{-1} with a capacity fade rate of 1.30% per day for 500 cycles, a Coulombic efficiency of ~99.8%, and an energy efficiency of 87%. Interestingly, the O_2 responsive behaviors of high-concentration AAOFBs distinctly differ from those of low-concentration AAOFBs. When the O_2 content increased from 10 to 100 ppm, the AAOFB with 0.5 M $[(NH_2Pr)(NH_3Pr)V]Cl_3$ did not have obvious capacity variations and still maintained the Coulombic efficiency of ~99.8% (Fig. 5). Consequently, the high-concentration AAOFB can stably operate in the high O_2 content of 100 ppm with a low capacity fade rate of 0.68% per d from 61th to 500th cycle. This is because the rate of electron transfer from the electrode surface to bipyridinium is more favorable than that to oxygen [34]. Thus, at high concentrations, such as 0.5 M or above, the reduction of dissolved oxygen becomes negligible. Moreover, the tendency of bipyridinium radicals to form larger π-dimers or molecular aggregates at high concentrations can also suppress O_2-induced side reactions, thereby enabling stable cycling of AAOFBs in high O_2 content environments. Therefore, the high concentration pH-decoupling AAOFB was able to stably run for long duration under relatively low N_2 purity (99.99%).

Indeed, bipyridinium compounds are highly toxic, stable in water, and have a long half-life in natural environments, posing a significant threat to mammalian health. However, when bipyridinium electrolytes are securely sealed in the tank with no leaks, the AOFBs should be technically safe. In addition, bipyridinium molecules are usually used in neutral or weakly alkaline electrolytes, which have low corrosiveness

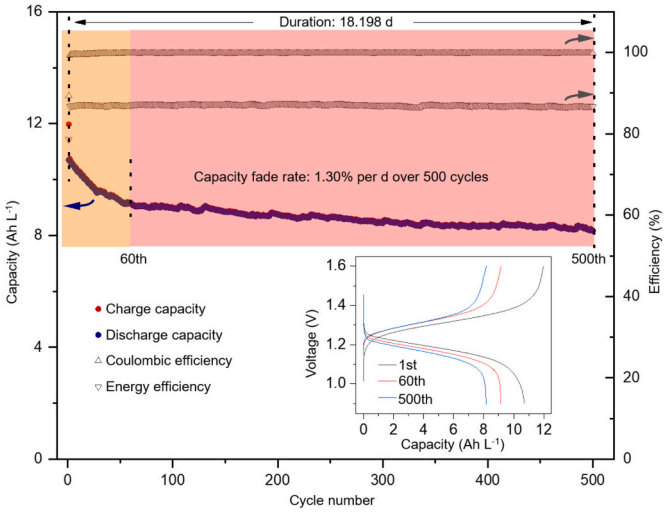

Fig. 5. High-concentration cycling performance with the charging cut-off voltage of 1.6 V via N_2 content control, showing charge capacity, discharge capacity, Coulombic efficiency and energy efficiency vs cycle number. Orange region: in N_2 99.999%. Red region: in N_2 99.99%. Inset: typical galvanostatic charge-discharge profiles. Conditions: anolyte, 5 mL of 0.5 M $[(NH_2Pr)(NH_3Pr)V]Cl_3$ in 2.0 M NaCl solution; catholyte, 7.5 mL of 0.5 M [TMP-TEMPO]Cl_2 in 2.0 M NaCl solution; current density, 20 mA cm^{-2}.

towards storage tanks, ensuring their long-term use in the sealed environment. Even if bipyridinium compounds leak from the AOFB systems into the environment, alkaline hydrogen peroxide, a nucleophilic oxidant, can act as an environmentally friendly detoxifier by disrupting the bipyridyl structures of bipyridiniums and converting them into low-toxicity or non-toxic products (Scheme S1).

4. Conclusions

In summary, we tackled a significant challenge in pH-decoupling AAOFBs by utilizing a molecular engineering approach to restricting the transport of proton and hydroxide ions across a commercially available conventional membrane. As a proof of concept, stable single-membrane pH-decoupling aqueous organic flow batteries were successfully constructed. The regulation of Coulomb repulsion and π-dimerization is flexible and dynamic by varying the charges through the protonation and deprotonation of amino terminals with simply adding an acid or base. When these proton-switchable bipyridiniums such as $[(NH_2Pr)(NH_3Pr)V]Cl_3$ were paired with TMP-TEMPO, the pH-decoupling AAOFB at low electrolyte concentration enables stable battery performance with a low capacity fade rate of 0.22% per d over 638 cycles, and high energy efficiency of ~88% and Coulombic efficiency of ~100%. Moreover, the high concentration pH-decoupling AAOFB demonstrated a practical capacity of ~10.7 Ah L^{-1} with a capacity fading rate of 0.047% per cycle upon 500 cycles (1.30% per day). Different from low concentration AAOFBs, the high concentration AAOFBs exhibited O_2 tolerant behavior and enabled a stable cycling performance at high O_2 content for long duration (more than 18 days). By regulating the atmospheric O_2 content, the O_2 impact on battery performance was well understood. Furthermore, the design approach can be readily applied to various pH-decoupling AAOFBs by using redox organics functionalized with NH_2 or NH_3^+ groups as anolytes and neutral redox organics as catholytes. We anticipate that this work will pave a novel and useful way for stable single-membrane pH-decoupling flow batteries.

CRediT authorship contribution statement

Mingguang Pan: Writing – review & editing, Writing – original

draft, Validation, Methodology, Investigation, Data curation, Conceptualization. **Zhong Jin:** Writing – review & editing, Resources, Methodology. **Jianwei Sun:** Writing – review & editing, Resources, Methodology. **Zhihu You:** Validation, Methodology. **Alan Y.L. Fan:** Validation, Methodology. **Minhua Shao:** Writing – review & editing, Writing – original draft, Validation, Supervision, Software, Resources, Project administration, Methodology, Investigation, Funding acquisition, Formal analysis, Data curation, Conceptualization.

Declaration of competing interest

The authors declare that they have no known competing financial interests or personal relationships that could have appeared to influence the work reported in this paper.

Acknowledgements

This work is fully supported by a grant from the Research Grants Council of the Hong Kong Special Administrative Region, China (Projects No. T23-601/17-R and JLFS/P-602/24), and Guangzhou Science and Technology Bureau (2024A03J0609).

Appendix A. Supplementary data

Supplementary data to this article can be found online at https://doi.org/10.1016/j.cej.2026.178913.

Data availability

Data will be made available on request.

References

[1] B. Dunn, H. Kamath, J.M. Tarascon, Electrical energy storage for the grid: a battery of choices, Science 334 (2011) 928–935.
[2] Y.X. Yao, J.F. Lei, Y. Shi, F. Ai, Y.C. Lu, Assessment methods and performance metrics for redox flow batteries, Nat. Energy 6 (2021) 582–588.
[3] G.L. Soloveichik, Flow batteries: current status and trends, Chem. Rev. 115 (2015) 11533–11558.
[4] Y. Xu, Y. Wen, J. Cheng, Y. Yang, Z. Xie, G. Cao, Novel organic redox flow batteries using soluble quinonoid compounds as positive materials, in: World Non-Grid-Connected Wind Power and Energy Conference (WNWEC 2009), IEEE, Nanjing China, 2009, pp. 1–4.
[5] B. Yang, L. Hoober-Burkhardt, F. Wang, G.K. Surya Prakash, S.R. Narayanan, An inexpensive aqueous flow battery for large-scale electrical energy storage based on water-soluble organic redox couples, J. Electrochem. Soc. 161 (2014) A1371–A1380.
[6] K. Lin, Q. Chen, M.R. Gerhardt, L. Tong, S.B. Kim, L. Eisenach, A.W. Valle, D. Hardee, R.G. Gordon, M.J. Aziz, M.P. Marshak, Alkaline quinone flow battery, Science 349 (2015) 1529–1532.
[7] T. Janoschka, N. Martin, U. Martin, C. Friebe, S. Morgenstern, H. Hiller, M. D. Hager, U.S. Schubert, An aqueous, polymer-based redox-flow battery using non-corrosive, safe, and low-cost materials, Nature 527 (2015) 78–81.
[8] M. Hu, W. Wu, J. Luo, T.L. Liu, Desymmetrization of viologen anolytes empowering energy dense, ultra stable flow batteries toward long-duration energy storage, Adv. Energy Mater. 12 (2022) 2202085.
[9] Z. Xiang, W. Li, K. Wan, Z. Fu, Z. Liang, Aggregation of electrochemically active conjugated organic molecules and its impact on aqueous organic redox flow batteries, Angew. Chem. Int. Ed. 62 (2023) e202214601.
[10] Z. Xiang, T. Ren, M. Huang, W. Li, L. Wang, K. Wan, Z. Fu, Z. Liang, Manipulating aggregate electrochemistry for high-performance organic redox flow batteries, Angew. Chem. Int. Ed. 64 (2025) e202416184.
[11] Z. Zhao, T. Li, C. Zhang, M. Zhang, S. Li, X. Li, Air-stable naphthalene derivative-based electrolytes for sustainable aqueous flow batteries, Nat. Sustainability 7 (2024) 1273–1282.
[12] G. Ge, F. Li, M. Yang, Z. Zhao, G. Hou, C. Zhang, X. Li, In situ molecular reconfiguration of pyrene redox-active molecules for high-performance aqueous organic flow batteries, Adv. Mater. 36 (2024) 2412197.
[13] X.-L. Lv, P. Sullivan, H.-C. Fu, X. Hu, H. Liu, S. Jin, W. Li, D. Feng, Dextrosil-viologen: a robust and sustainable anolyte for aqueous organic redox flow batteries, ACS Energy Lett. 7 (2022) 2428–2434.
[14] W. Lee, G. Park, Y. Kwon, Alkaline aqueous organic redox flow batteries of high energy and power densities using mixed naphthoquinone derivatives, Chem. Eng. J. 386 (2020) 123985.
[15] X. Li, P. Gao, Y.-Y. Lai, J.D. Bazk, H.-Y. Lin, V. Murugesan, S. Zhang, C.-F. Cheng, W.-Y. Tung, Y.-T. Lai, R. Feng, J. Wang, C.-L. Wang, W. Wang, Y. Zhu, Symmetry-breaking design of an organic iron complex catholyte for a long cyclability aqueous organic redox flow battery, Nat. Energy 6 (2021) 873–881.
[16] G.S. Nambafu, K. Siddharth, C. Zhang, T. Zhao, Q. Chen, K. Amine, M. Shao, An organic bifunctional redox active material for symmetric aqueous redox flow battery, Nano Energy 89 (2021) 106422.
[17] J. Huang, Z. Yang, V. Murugesan, E. Walter, A. Hollas, B. Pan, R.S. Assary, I. A. Shkrob, X. Wei, Z. Zhang, Spatially constrained organic diquat anolyte for stable aqueous flow batteries, ACS Energy Lett. 3 (2018) 2533–2538.
[18] F. Ai, Z.Y. Wang, N.C. Lai, Q.L. Zou, Z.J. Liang, Y.C. Lu, Heteropoly acid negolytes for high-power-density aqueous redox flow batteries at low temperatures, Nat. Energy 7 (2022) 417–426.
[19] J. Xu, S. Pang, X. Wang, P. Wang, Y. Ji, Ultrastable aqueous phenazine flow batteries with high capacity operated at elevated temperatures, Joule 5 (2021) 2437–2449.
[20] S. Huang, H. Zhang, M. Salla, J. Zhuang, Y. Zhi, X. Wang, Q. Wang, Molecular engineering of dihydroxyanthraquinone-based electrolytes for high-capacity aqueous organic redox flow batteries, Nat. Commun. 13 (2022) 4746.
[21] A. Hollas, X. Wei, V. Murugesan, Z. Nie, B. Li, D. Reed, J. Liu, V. Sprenkle, W. Wang, A biomimetic high-capacity phenazine-based anolyte for aqueous organic redox flow batteries, Nat. Energy 3 (2018) 508–514.
[22] D.G. Kwabi, Y. Ji, M.J. Aziz, Electrolyte lifetime in aqueous organic redox flow batteries: a critical review, Chem. Rev. 120 (2020) 6467–6489.
[23] B. Hu, C. DeBruler, Z. Rhodes, T.L. Liu, Long-cycling aqueous organic redox flow battery (AORFB) toward sustainable and safe energy storage, J. Am. Chem. Soc. 139 (2017) 1207–1214.
[24] L. Zhang, R. Feng, W. Wang, G. Yu, Emerging chemistries and molecular designs for flow batteries, Nat. Rev. Chem. 6 (2022) 524–543.
[25] Q. Chen, Y. Lv, Z. Yuan, X. Li, G. Yu, Z. Yang, T. Xu, Organic electrolytes for pH-neutral aqueous organic redox flow batteries, Adv. Funct. Mater. 32 (2022) 2108777.
[26] J.D. Griffin, A.R. Pancoast, M.S. Sigman, Interrogation of 2,2′-bipyrimidines as low-potential two-electron electrolytes, J. Am. Chem. Soc. 143 (2021) 992–1004.
[27] G. Yang, Y. Zhu, Z. Hao, Q. Zhang, Y. Lu, Z. Yan, J. Chen, An aqueous all-quinone-based redox flow battery, Adv. Energy Mater. 14 (2024) 2400022.
[28] Y. Liu, P. Zhang, Z. Wu, J. Wei, G. Ding, X. Song, J. Ma, W. Wang, Z. Jin, Screening ultra-stable (phenazine)dioxyalkanocic acids with varied water-solubilizing chain lengths for high-capacity aqueous redox flow batteries, J. Am. Chem. Soc. 146 (2024) 3293–3302.
[29] M. Pan, Z. Jin, T. Zhao, J. Sun, Z. You, E.P. Delmo, M. Farhadpour, Z. Wu, M. Shao, Highly soluble and crossover-free all-organic redox pair using *N*-heterocycle-linked TEMPO and two-electron-capable bipyridinium towards high performance aqueous flow batteries, Chem. Eng. J. 496 (2024) 153504.
[30] D. Xi, A.M. Alfaraidi, J. Gao, T. Cochard, L.C.I. Faria, Z. Yang, T.Y. George, T. Wang, R.G. Gordon, R.Y. Liu, M.J. Aziz, Mild pH-decoupling aqueous flow battery with practical pH recovery, Nat. Energy 9 (2024) 479–490.
[31] M. Park, E.S. Beh, E.M. Fell, Y. Jing, E.F. Kerr, D.D. Porcellinis, M.-A. Goulet, J. Ryu, A.A. Wong, R.G. Gordon, J. Cho, M.J. Aziz, A high voltage aqueous zinc–organic hybrid flow battery, Adv. Energy Mater. 9 (2019) 1900694.
[32] M. Pan, L. Gao, J. Liang, P. Zhang, S. Lu, Y. Lu, J. Ma, Z. Jin, Reversible redox chemistry in pyrrolidinium-based TEMPO radical and extended viologen for high-voltage and long-life aqueous redox flow batteries, Adv. Energy Mater. 12 (2022) 2103478.
[33] E.S. Beh, D.D. Porcellinis, R.L. Gracia, K.T. Xia, R.G. Gordon, M.J. Aziz, A neutral pH aqueous organic–organometallic redox flow battery with extremely high capacity retention, ACS Energy Lett. 2 (2017) 639–644.
[34] M.E. Carrington, K. Sokołowski, E. Jónsson, E.W. Zhao, A.M. Graf, I. Temprano, J. A. McCune, C.P. Crey, O.A. Scherman, Associative pyridinium electrolytes for air-tolerant redox flow batteries, Nature 623 (2023) 949–955.
[35] Z. Peng, Z. Ren, S. Chen, Y. Zhao, P. Jannasch, J. Yang, Flexibly linked and isomeric piperidinium-based anion exchange membrane with enhanced alkaline stability for durable alkaline water electrolysis, Int. J. Hydrog Energ. 188 (2025) 151884.
[36] Q. Wang, T. Wei, Z. Peng, Y. Zhao, P. Jannasch, J. Yang, High-performance anion exchange membranes based on poly(oxindole benzofuran dibenzo-18-crown-6)s functionalized with hydroxyl and quaternary ammonium groups for alkaline water electrolysis, J. Colloid Interface Sci. 686 (2025) 304–317.
[37] Z. Peng, R. Zhang, W. Zhao, Y. Wu, Y. Zhao, J. Yang, Triazine-based multi-heteroatom branching strategy for high-performance anion exchange membranes in water electrolysis, J. Membr. Sci. 738 (2026) 124827.